

Radiative cooling of a spin ensemble

B. Albanese,¹ S. Probst,¹ V. Ranjan,¹ C. Zollitsch,² M. Pechal,³ A. Wallraff,³
J.J.L. Morton,² D. Vion,¹ D. Esteve,¹ E. Flurin,¹ and P. Bertet*¹

¹Quantronics group, SPEC, CEA, CNRS, Université Paris-Saclay, CEA Saclay 91191 Gif-sur-Yvette Cedex, France

²London Centre for Nanotechnology, University College London, London WC1H 0AH, United Kingdom

³Department of Physics, ETH Zurich, CH-8093 Zurich, Switzerland

Physical systems reach thermal equilibrium through energy exchange with their environment, and for spins in solids the relevant environment is almost always the host lattice in which they sit. However, recent studies motivated by observations from Purcell showed how coupling to a cavity can become the dominant form of relaxation for spins, given suitably strong spin-cavity coupling. In this regime, the cavity electromagnetic field takes over from the lattice as the dominant environment, inviting the prospect of controlling the spin temperature independently from that of the lattice, by engineering a suitable cavity field. Here, we report on precisely such control over spin temperature, illustrating a novel and universal method of electron spin hyperpolarisation. By switching the cavity input between loads at different temperatures we can control the electron spin polarisation, cooling it below the lattice temperature. Our demonstration uses donor spins in silicon coupled to a superconducting micro-resonator and we observe an increase of spin polarisation of over a factor of two. This approach provides general route to signal enhancement in electron spin resonance, or indeed nuclear magnetic resonance through dynamical nuclear spin polarisation (DNP).

When a physical system is coupled to several reservoirs at different temperatures, it equilibrates at an intermediate temperature which depends on the strength with which it is coupled to each bath. An electron spin in a solid is coupled to two different reservoirs: phonons in its host lattice, and microwave photons in its electromagnetic environment. The strength of this coupling is characterized by the rate at which the spin, of Larmor frequency ω_{spin} , relaxes by spontaneously emitting a quantum of energy $\hbar\omega_{\text{spin}}$ into each bath. In usual magnetic resonance experiments [5], the spin-lattice relaxation rate Γ_{phon} is many orders of magnitude larger than the radiative relaxation rate Γ_{phot} , so that the spin temperature T_{spin} is determined by the sample temperature T_{phon} regardless of the temperature of the microwave photons T_{phot} .

The strength of radiative relaxation can however be enhanced by coupling the spins resonantly to one mode of a microwave resonator of frequency $\omega_0 = \omega_{\text{spin}}$, as discovered by Purcell [2, 6, 7]. The coupling strength is then given by $\Gamma_{\text{phot}} = 4g^2/\kappa$, g being the spin-photon coupling constant and κ the resonator mode relaxation rate. Superconducting micro-resonators can be designed with a small mode volume, which increases g , while retaining a high quality factor, which reduces κ . This makes it possible to reach the *Purcell regime* defined by $\Gamma_{\text{phot}} \gg \Gamma_{\text{phon}}$, as demonstrated in recent experiments [1]. In this regime, T_{spin} should thus be equal to T_{phot} and no longer to T_{phon} , and electron spin hyperpolarisation should be possible by cooling the microwave field down to a temperature $T_{\text{phot}} \ll T_{\text{phon}}$. The simplest way to do so is to connect the resonator input to a cold 50 Ω resistor, as shown in Fig. 1a. As long as the coupling rate of the resonator field κ_{ext} to this cold reservoir at temperature T_{cold} is larger than the coupling rate $\kappa_{\text{int}} = \kappa - \kappa_{\text{ext}}$ to the hot reservoir consisting of its internal losses at temperature T_{int} , the resonator field temperature is lowered, which

in turn cools down the spins (see Fig. 1a). To infer T_{spin} , we use the fact that the amplitude of a spin-echo is proportional to $(N_{\uparrow} - N_{\downarrow}) \equiv \Delta N$, N_{\uparrow} and N_{\downarrow} being the number of spins in the excited and ground states, respectively. For an ensemble of $N = N_{\uparrow} + N_{\downarrow}$ spin-1/2 systems, $\Delta N = Np(T_{\text{spin}})$ with $p(T_{\text{spin}}) = \tanh(\hbar\omega_{\text{spin}}/2kT_{\text{spin}})$ the temperature-dependent spin polarisation [8].

Another key measurable quantity is the rate Γ_1 at which the spins return to thermal equilibrium. In the Purcell regime, this rate $\Gamma_1 = [2\bar{n}(T_{\text{phot}}) + 1]\Gamma_{\text{phot}}$ is expected to be temperature-dependent because the rate of absorption and stimulated emission of microwave photons by each spin depends on the average intra-resonator thermal photon number $\bar{n}(T_{\text{phot}}) = 1/[1 - e^{-\hbar\omega_0/kT_{\text{phot}}}]$ [6, 9, 10]. Noting that $1/[2\bar{n}(T_{\text{phot}}) + 1] = \tanh(\hbar\omega_{\text{spin}}/2kT_{\text{phot}})$ we thus expect $\Gamma_1(T_{\text{phot}})/\Gamma_1(0) = p(0)/p(T_{\text{phot}}) = [2\bar{n}(T_{\text{phot}}) + 1]$ in the Purcell regime, an interesting prediction that we test in this work.

This radiative spin cooling scheme requires that across the temperature range between T_{cold} and T_{phon} , spins are in the Purcell regime ($\Gamma_{\text{phot}} \gg \Gamma_{\text{phon}}$), and the resonator is over-coupled ($\kappa_{\text{ext}} \gg \kappa_{\text{int}}$). Here we use the electron spin of donors in silicon, which have low spin-lattice relaxation rate $\Gamma_{\text{phon}} \sim 10^{-4} - 10^{-3} \text{ s}^{-1}$ below 1 K at 5–10 GHz [11, 12], coupled to a superconducting micro-resonator in niobium, whose internal losses κ_{int} are very low in the same temperature interval, to demonstrate radiative spin cooling from $T_{\text{phon}} \sim 0.85 \text{ K}$ using a cold load at $T_{\text{cold}} = 20 \text{ mK}$.

The device geometry is depicted in Fig. 1c. The niobium resonator consists of an inter-digitated capacitor shunted by a 2 μm -wide inductive wire. It is patterned on top of a silicon substrate in which bismuth atoms were implanted over a $\sim 1 \mu\text{m}$ depth. A dc magnetic field B_0 is applied parallel to the sample surface, along the inductor (z axis), to tune

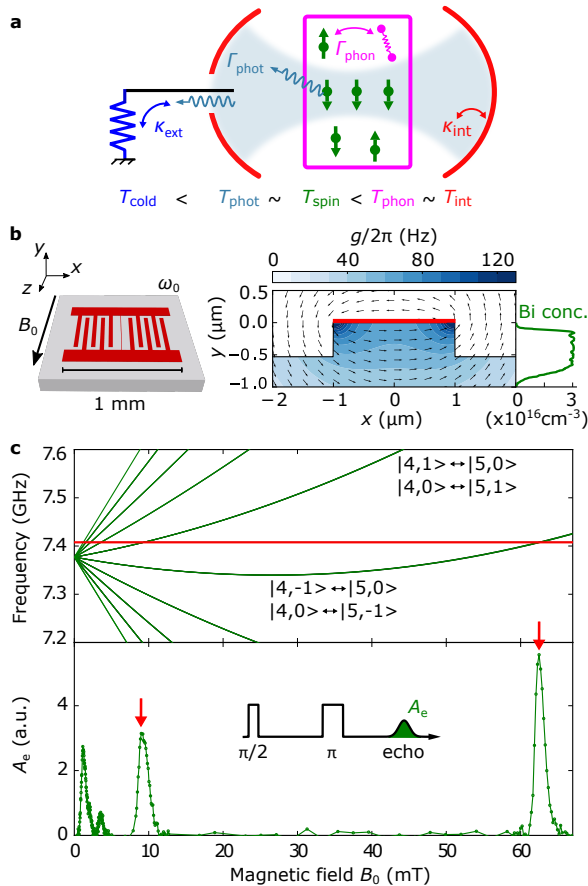


FIG. 1. Radiative spin cooling principle, and energy spectrum of Bi donors in silicon. **a**, Principle of the experiment. Spins (green) in a crystal (magenta) are coupled both to a bath of phonons at temperature T_{phon} with a rate Γ_{phon} , and to a bath of microwave photons at a temperature T_{phot} with a rate Γ_{phot} , which determines their equilibrium temperature T_{spin} . The temperature of the photons T_{phot} is in turn determined by their coupling with rate κ_{int} to the cavity internal losses at temperature T_{int} and with rate κ_{ext} to the load located at the cavity input. When this load is placed at a low temperature T_{cold} , the intra-cavity field is radiatively cooled provided $\kappa_{\text{ext}} \gg \kappa_{\text{int}}$, and the spins are cooled in turn if $\Gamma_{\text{phot}} \gg \Gamma_{\text{phon}}$. **b**, Left, a 50 nm thick niobium superconducting resonator (red) of frequency ω_0 is fabricated on a silicon chip where bismuth atoms are implanted. A static magnetic field B_0 is applied parallel to the central inductor wire of the resonator. Right, device cross section around the inductor wire (red). The spin-photon coupling constant g (color code) is represented in the Bi-doped region together with the normalized B_1 field vector (arrows) generated by the inductor current. **c**, Top, Solid green lines are calculated electron spin resonance transitions of the bismuth donors. The resonator frequency $\omega_0/2\pi = 7.408$ GHz (red line) is resonant with 6 transitions in the 0-70 mT range. (Bottom) Measured spin-echo amplitude A_e as a function of B_0 (blue dots), showing the expected transitions.

the spin resonance by Zeeman effect. The resonator inductance generates a spatially inhomogeneous microwave magnetic field B_1 , which results in a spatial dependence of the spin-resonator coupling constant g shown in Fig. 1b (see also Methods). This leads to a variation of the spin rotation angles and also relaxation rates Γ_{phot} throughout the sample, which are taken into account in the simulations discussed below.

The donor spin Hamiltonian $H = -\gamma_e B_0 S_z + \mathbf{A} \mathbf{S} \cdot \mathbf{I}$ describes the Zeeman shift of the $S = 1/2$ electron spin of the donor with a gyromagnetic ratio $\gamma_e/2\pi = 28$ GHz/T and its hyperfine interaction of strength $A/2\pi = 1.45$ GHz with the nuclear spin $I = 9/2$ of the bismuth atom [13, 14]. In the low-field regime $\gamma_e B_0 \lesssim A$, the 20 energy eigenstates are hybridized electro-nuclear spin states, characterized by the eigenvalues F of the total angular momentum $\mathbf{F} = \mathbf{I} + \mathbf{S}$ and m of its projection along z , F_z . They can be grouped into a $F = 4$ ground state manifold of 9 states and a $F = 5$ excited state manifold of 11 states, separated by ~ 7.38 GHz (see Methods). All $\Delta m = \pm 1$ transitions are allowed in this regime; the dependence of their frequency on B_0 is shown in Fig. 1c. Corresponding peaks are observed in an echo-detected field sweep (see Fig. 1c). Data in the following are obtained either at $B_0 = 62.5$ mT on the quasi-degenerate $|F = 4, m = -1\rangle \leftrightarrow |5, 0\rangle$ and $|4, 0\rangle \leftrightarrow |5, -1\rangle$ transitions, or at $B_0 = 9.5$ mT on the seemingly quasi-degenerate $|4, 1\rangle \leftrightarrow |5, 0\rangle$ and $|4, 0\rangle \leftrightarrow |5, 1\rangle$ transitions, and we treat each one in the following as an approximate effective spin-1/2 system (see Methods).

In a first experiment, we measure the spin polarization p and relaxation time Γ_1^{-1} as a function of the temperature T , in a setup ensuring that $T_{\text{phot}} = T_{\text{phon}} = T_{\text{spin}} = T_{\text{int}} = T$ (see Fig. 2a). As shown in Fig. 2b, we first apply a π pulse to excite the spins, let them relax during a varying time Δt , and finally measure a Hahn echo whose integral A_e is proportional to $\Delta N(\Delta t) = Np(T_{\text{spin}})(1 - 2e^{-\Gamma_1^{-1}\Delta t})$, a pulse sequence known as inversion recovery [5]. Echo curves are shown in Fig. 2b for $\Delta t \ll \Gamma_1^{-1}$ and $\Delta t \gg \Gamma_1^{-1}$, measured at $T = 20$ mK. The phase of the short- Δt echo is inverted with respect to the long- Δt echo, as expected. The shape of the short- Δt echo is due to the dependence of the Rabi angle on detuning and is well reproduced by simulations (see Fig. 2b). Figure 2b shows $A_e(\Delta t)$ at 20 mK. The curve is well fitted by an exponential decay of time constant $\Gamma_1^{-1} = 5.9$ s (dashed curve), and in excellent agreement with a complete simulation of the experiment that considers Purcell relaxation without any adjustable parameter (solid green curve), confirming that the donors are in the Purcell regime at 20 mK. We measure $A_e(\Delta t)$ for varying temperatures T ; an exponential fit then yields both the relaxation time $\Gamma_1^{-1}(T)$ as well as the steady-state spin-echo area $A_e(T)$. Both quantities are shown in Fig. 2c, with a scale evidencing their similar temperature dependence, in quantitative agreement with the expected $1/[2\bar{n}(T) + 1]$ dependence. This demonstrates that the bismuth donor spins are in the Purcell regime at least up to 1 K.

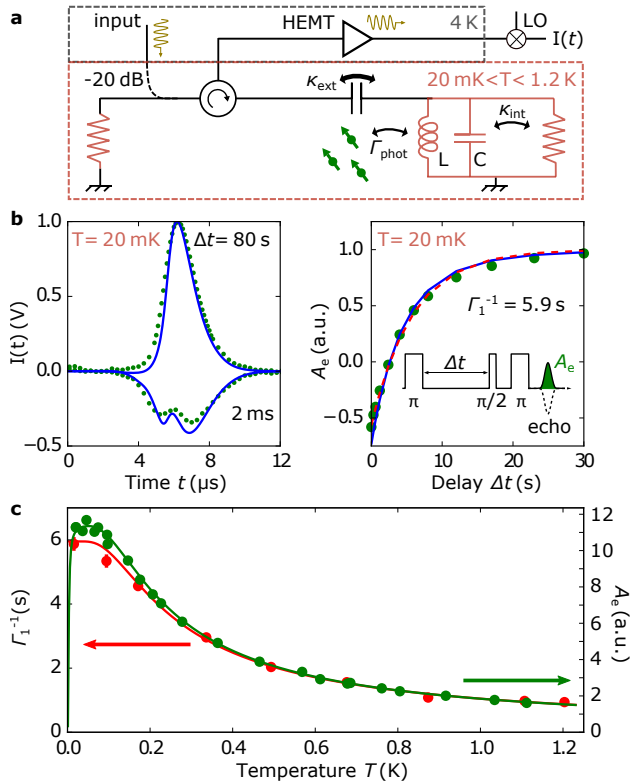


FIG. 2. Temperature dependence of spin relaxation rate and polarization. **a**, Setup schematics. The spins, the LC resonator to which they are coupled, and the cold load are all thermalized to the same temperature T . Microwave pulses are sent to the cavity input via a -20 dB coupler. The reflected signal, with the spin-echo, is amplified at 4 K by a High-Electron-Mobility-Transistor amplifier (HEMT) and demodulated at room-temperature, yielding the time-dependent quadrature $I(t)$. **b**, Measured (green dots) and simulated (blue line) echo signals (left panel) at short and long Δt , as well as integrated echo A_e (right panel) as a function of Δt , both at $T = 20$ mK and $B_0 = 62.5$ mT. The pulse sequence is shown in the right panel. The red dashed curve is an exponential fit with $\Gamma_1^{-1} = 5.9$ s. **c**, Measured relaxation time Γ_1^{-1} (red dots) and integrated echo A_e (green dots) as a function of temperature T , at $B_0 = 62.5$ mT. The detailed measurement procedure is explained in the Methods. Red curve is a fit to the $\Gamma_1^{-1}(T)$ data between 0.3 K and 1 K using the function $\Gamma_f^{-1}/[2\bar{n}(T) + 1]$, with Γ_f^{-1} as adjustable parameter. Green curve is a fit to the $A_e(T)$ data between 0.3 K and 1 K using the function $A_f\Delta N(T)$, where $\Delta N(T)$ is the expected population difference for the transition considered and A_f is the adjusted parameter. The green curve deviates from the red below 0.2 K due to the 20 levels of the bismuth donor system.

The setup for radiative spin cooling is depicted in Fig. 3a. The device is now thermally anchored at the still stage of the dilution refrigerator, so that $T_{\text{phon}} = 0.85$ K. We use an electromechanical switch to connect the resonator input, via a superconducting coaxial cable, to a 50Ω resistor thermal-

ized either also at the still stage (*hot* configuration), i.e. at T_{phon} or at the mixing chamber of the cryostat (*cold* configuration, $T_{\text{cold}} = 20$ mK). The field leaking from or reflected onto the cavity is routed via a circulator (also anchored at the still temperature) towards the detection chain where it is first amplified by a Josephson Travelling-Wave Parametric Amplifier [15]. Microwave control pulses are sent into the cavity via a 20 dB directional coupler. This ensures that the temperature of the microwave radiation field incident onto the resonator, and therefore T_{phot} , is dominantly determined by the switch setting.

We first estimate the temperature $T_{\text{phot}}^{\text{cold}}$ of the intra-cavity field when the switch is connected to the cold load, using a series of noise measurements described in the Methods section, similar to recent work [16, 17]. We obtain $T_{\text{phot}}^{\text{cold}} = 500 \pm 60$ mK, proving that the microwave field is indeed cooled radiatively, but that this cooling is only partial, which we attribute to the presence of microwave losses α in-between the cold load and the resonator at the temperature T_{phon} (see Methods).

Hahn-echoes are then measured for the two different switch settings, under otherwise identical conditions (drive pulse amplitude, and repetition time). As seen in Fig. 3b, the echo amplitude more than doubles when the resonator is connected to the cold load, which demonstrates radiative spin hyperpolarization with $\eta \equiv p^{\text{cold}}/p^{\text{hot}} = 2.3 \pm 0.1$. We also measure Γ_1^{-1} in the two switch configurations, and find that $\Gamma_1^{\text{hot}}/\Gamma_1^{\text{cold}} = \eta$, as expected. Contrary to the energy relaxation time, the coherence time T_2 is not affected by the switch settings, as demonstrated in Fig. 3c which shows $A_e(2\tau)$ for both configurations. The decay is Gaussian in both cases, with a characteristic time $T_2 = 600 \mu\text{s}$, due to spectral diffusion in the bath of ^{29}Si nuclear spins [13, 18]. This confirms that the change in echo amplitude in Fig. 3b is due to enhanced spin polarization, rather than to a change in T_2 .

The measured cooling efficiency $\eta = 2.3$ corresponds to a spin temperature $T_{\text{spin}}^{\text{cold}} = 350 \pm 10$ mK, which is close to (or even slightly lower than) the field temperature $T_{\text{phot}}^{\text{cold}}$ estimated from noise measurements. This proves that spin-lattice relaxation is not the factor limiting the spin cooling, and that the spins thermalize to the temperature of their electromagnetic environment within the accuracy of the experiment. The spin temperature achieved is explained by $\alpha = 0.23 \pm 0.03$, corresponding to 1.15 ± 0.15 dB loss at 850 mK, a plausible value for the combined effect of circulator insertion losses, directional coupler contribution, and possible spurious reflections due to impedance mismatch in the line.

The sensitivity enhancement obtained by radiative spin hyperpolarization does not scale like η as in other hyperpolarization schemes such as DNP but only as $\sqrt{\eta}$, because the optimal waiting time t_{rep} between subsequent experimental sequences, which is of order Γ_1^{-1} , also scales as η , as seen

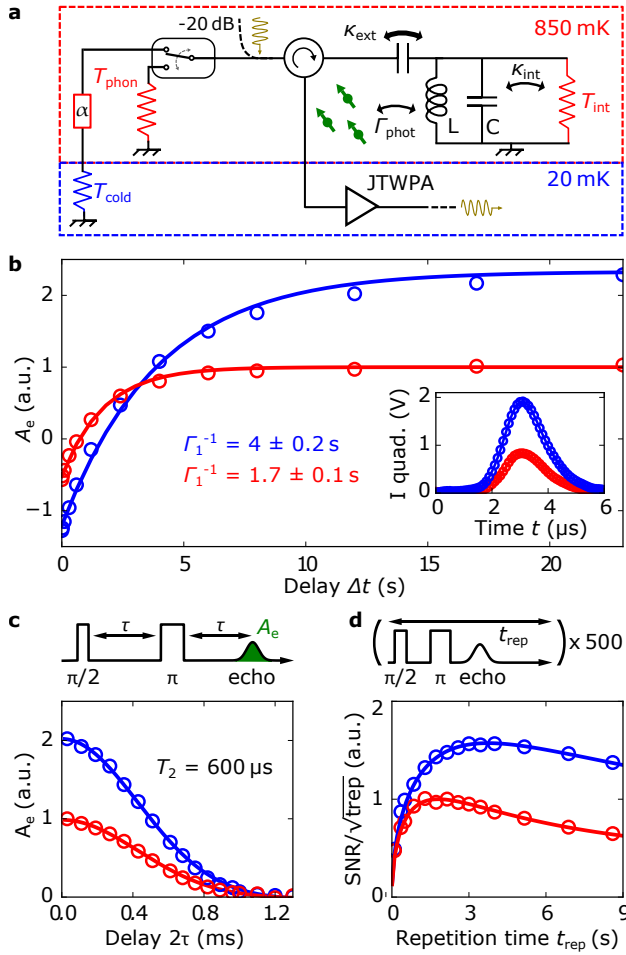


FIG. 3. **Radiative cooling demonstration** **a**, Simplified equivalent electrical circuit. The spins and resonator are thermally anchored at $T_{\text{phon}} = 0.85$ K. The resonator input is connected to an electromechanical switch that can either be connected to a hot (T_{phon}) or cold (T_{cold}) $50\ \Omega$ load. The output signal is routed via a circulator towards a Josephson Traveling-Wave Amplifier (JTWPA) installed at 20 mK. Excitation microwave pulses are sent via a -20 dB directional coupler. **b**, (inset) Measured spin-echo signal showing a $\eta = 2.3$ increase in amplitude in the *cold* configuration. (Main panel) Measurements (open circles) and exponential fits (solid lines) of the integrated echo area A_e as a function of the waiting time Δt of the inversion recovery pulse sequence shown in Fig. 2b, yielding $\Gamma_1^{-1} = 4 \pm 0.2$ s (*cold*) and $\Gamma_1^{-1} = 1.7 \pm 0.1$ s (*hot*). **c**, Measurements (open circles) and Gaussian fits (solid lines) of the integrated echo A_e as a function of waiting time τ in a Hahn echo sequence (top), yielding $T_2 = 600\ \mu\text{s}$ in both switch configurations. **d**, Measured (open circles) signal-to-noise ratio SNR, obtained by dividing the mean value of 500 echo samples by their standard deviation, as a function of the repetition time t_{rep} (see pulse sequence on top), for both switch configurations. Solid lines are fit with $p(1 - e^{-\Gamma_1^{-1} t_{\text{rep}}})/(\bar{\sigma} \sqrt{t_{\text{rep}}})$, where $\bar{\sigma}$ is the mean of all the σ_e and p is the equilibrium polarization, yielding $\eta = \Gamma_1^{\text{hot}}/\Gamma_1^{\text{cold}} = p^{\text{cold}}/p^{\text{hot}} = 2.1$. In all panels red and blue represent data or models in the *hot* and *cold* switch configuration, respectively.

above. We demonstrate this by measuring the mean value and standard deviation of A_e for 500 echo traces as a function of the repetition time t_{rep} (see Fig. 3d). The highest sensitivity is obtained for $t_{\text{rep}} \approx 1.25[\Gamma_1^{\text{cold,hot}}]^{-1}$, both in the *cold* and the *hot* load cases. It is 1.6 times larger in the *cold* than in the *hot* configuration, slightly larger than $\sqrt{\eta} = 1.52$ because switching to the cold load also substantially reduces the effective noise temperature of our detection chain (by 7%).

The presence of an additional non-radiative coupling of the spins with rate Γ_{phon} to a bosonic bath of temperature T_{phon} should enter in competition with radiative cooling, and therefore reduce its efficiency to $\eta = \Gamma_1^{\text{hot}}/\Gamma_1^{\text{cold}}$, with $\Gamma_1^{\text{cold,hot}} = \Gamma_{\text{phon}}[2\bar{n}(T_{\text{phon}}) + 1] + \Gamma_{\text{phot}}[2\bar{n}(T_{\text{phot}}^{\text{cold,hot}}) + 1]$.

We test this prediction by controllably exciting carriers into the silicon conduction band, which are known to reduce the spin relaxation time of donors [11]. For this we irradiate the sample with infrared radiation at 950 nm emitted by a LED biased by a current I . The spin relaxation time Γ_1^{-1} , measured in the *hot* configuration, is indeed observed to decrease with I (see Fig. 4a), from which we determine $\Gamma_{\text{phon}}^{-1}(I)$. We then measure the cooling efficiency $\eta(I)$ (see Fig. 4a). At large LED powers, radiative spin cooling stops working as expected ($\eta \sim 1$), because spins relax dominantly by interaction with the charge carriers in the substrate, whose presence is unaffected by the switch settings. The $\eta(I)$ dependence predicted by our model agrees semi-quantitatively with the data. The ratio of relaxation times $\Gamma_1^{\text{hot}}(I)/\Gamma_1^{\text{cold}}(I)$ also closely follows the measured $\eta(I)$, as expected.

We finally investigate the spin polarization dynamics (see Fig. 4b). For that we replace the electromechanical switch with a superconducting device mounted at 20 mK, able to switch in a few nanoseconds without heating [19]. At 9.5 mT the area A_e of a Hahn echo is measured at delay Δt after the switch configuration is changed, either from *cold* to *hot* or vice-versa. The relaxation times in the two cases are expected to be the two values of $\Gamma_{\text{phot}}[2\bar{n}(T_{\text{phot}}^{\text{cold,hot}}) + 1]$ determined by the new thermal photon population after the switching. An exponential fit of the two curves gives $(\Gamma_1^{\text{hot}})^{-1} = 3.7$ s and $(\Gamma_1^{\text{cold}})^{-1} = 6.4$ s. The approximate equality of the two measured ratios, $\Gamma_1^{\text{hot}}/\Gamma_1^{\text{cold}} = 1.7$ and $p^{\text{cold}}/p^{\text{hot}} = 1.5$, is again in agreement with our model. The reduced η with respect to the previously presented result is explained by a measured 3dB insertion loss of the superconducting switch.

We now come to the limitations and potential real-world applications of our scheme. Cooling the spins while keeping the sample hot is useful in situations where large cooling powers are needed, for instance in spin-based microwave-optical transduction experiments which require large optical powers [20]. One limitation of the present scheme is that the lowest spin temperature that could possibly be reached (in a lossless setup) is the temperature T_{cold} at which the cold load is thermally anchored. However, one could also imag-

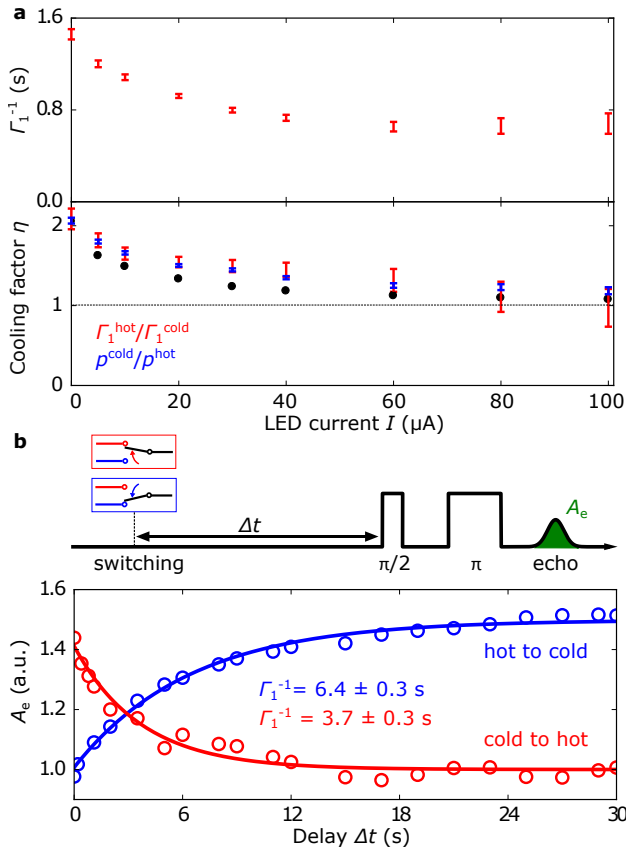


FIG. 4. **Suppression of cooling by carrier injection, and cooling dynamics.** **a**, (Top) Spin relaxation time Γ_1^{-1} , measured with an inversion recovery sequence in the *hot* configuration, as a function of the current I through the LED. (Bottom) Measured cooling factor η (blue) and $\Gamma_1^{\text{hot}}/\Gamma_1^{\text{cold}}$ (red) as a function of I . The black dots are the prediction of the model described in the main text. Error bars are estimated from the standard deviation of the exponential fit parameters. **b**, Measured integrated echo area A_e (open circles) at 9.5 mT as a function of the waiting time Δt between a rapid change of switch configuration and the echo sequence shown on top. Solid lines are exponential fits, yielding $\Gamma_1^{-1} = 6.4 \pm 0.3$ s from hot to cold (blue) and $\Gamma_1^{-1} = 3.7 \pm 0.3$ s from cold to hot (red).

ine cooling the resonator field using parametric processes in a circuit quantum electrodynamics platform, as recently demonstrated in [21]. This would enable to cool the resonator field and thus the spins to arbitrarily low temperatures, an appealing perspective for magnetic resonance. Such an active radiative cooling scheme could work even in ^4He cryostats with base temperature 1.5–4 K, as in standard low-temperature EPR spectrometers. Even higher operating temperatures could be envisioned by using high-Tc superconducting thin-films, although the microwave losses caused by quasiparticles may be an issue [22].

Regarding applications to magnetic resonance spec-

troscopy, we first note that to our knowledge the only other existing electron spin hyperpolarisation method is optical illumination, which requires spin systems with very specific level schemes [23–26], contrary to our method which only makes use of the spin transition. A broad set of Electron Paramagnetic Resonance (EPR) measurements (including field-sweeps, g-tensor measurements, HYSCORE, DEER and ENDOR etc.) could benefit from an increase in sensitivity of at least $\sqrt{\eta}$, translating into a measurement time shorter by a factor of η , obtained by radiative hyperpolarisation. Only those EPR studies where the spin-lattice relaxation rate is itself the object of interest would be excluded from this approach. Regarding suitable spin species, the key requirement is for the spins to be in the Purcell regime. At cryogenic temperatures, electron spin-lattice relaxation times $\Gamma_{\text{phon}}^{-1}$ are typically in the $10^{-3} - 10^3$ s range [27–29], so that a Purcell time $\Gamma_{\text{phot}}^{-1} \sim 10^{-2}$ s, which has already been demonstrated with a different resonator geometry [30], would be sufficient for many species. The method could also be fruitfully applied to the radicals used in DNP as polarizing agents, and might enable to obtain large nuclear spin enhancement factors in less demanding conditions than those usually required [4] (lower magnetic field, lower microwave frequency, or higher temperature).

We have shown that in the Purcell regime, the spin temperature is determined by the temperature of the microwave field and not of the sample itself. We have used this fundamental insight to demonstrate a novel electron spin hyperpolarisation method, which is effective for all spin systems provided they can reach the Purcell regime. Further work will aim at demonstrating active Purcell cooling, and investigate real-world applications of our method.

Acknowledgements We thank P. Sénat, D. Duet and J.-C. Tack for the technical support, and are grateful for fruitful discussions within the Quantronics group. We acknowledge IARPA and Lincoln Labs for providing a Josephson Traveling-Wave Parametric Amplifier. We acknowledge support of the European Research Council under the European Community’s Seventh Framework Programme (FP7/2007-2013) through grant agreement No. 615767 (CIRQUSS), of the Agence Nationale de la Recherche under the Chaire Industrielle NASNIQ, of the Région Ile-de-France via the DIM SIRTEQ, of the Engineering and Physical Sciences Research Council (EPSRC) through Grant No. EP/K025945/1, and of the Horizon 2020 research and innovation programme through grant agreement No. 771493 (LOQO-MOTIONS).

Author contributions B.A., S.P. and P.B. designed the experiment. J.J.L.M. and C.Z. provided and characterized the implanted silicon sample, on which B.A. and S.P. fabricated the niobium resonator. B.A. performed the measurements, with help from S.P. and V.R. B.A. and P.B. analyzed the data. B.A. and V.R. performed the simulations. M.P. realized and tested the superconducting switch in a project guided by A.W. B.A. and P.B. wrote the manuscript. S.P., V.R., A.W.,

J.J.L.M., D.V., D.E., and E.F. contributed with useful input to the manuscript.

-
- [1] A. Bienfait, J.J. Pla, Y. Kubo, X. Zhou, M. Stern, C.-C. Lo, C.D. Weis, T. Schenkel, D Vion, D. Esteve, J.J.L. Morton, and P. Bertet. Controlling Spin Relaxation with a Cavity. *Nature*, 531:74 – 77, 2016.
- [2] E. M Purcell. Spontaneous emission probabilities at radio frequencies. *Phys. Rev.*, 69(681), 1946.
- [3] A. Abragam and M. Goldman. Principles of dynamic nuclear polarisation. *Reports on Progress in Physics*, 41(3):395–467, March 1978.
- [4] Jan H. Ardenkjr-Larsen, Bjrñ Fridlund, Andreas Gram, Georg Hansson, Lennart Hansson, Mathilde H. Lerche, Rolf Servin, Mikkel Thaning, and Klaes Golman. Increase in signal-to-noise ratio of 10,000 times in liquid-state NMR. *Proceedings of the National Academy of Sciences*, 100(18):10158–10163, September 2003.
- [5] A. Schweiger and G. Jeschke. *Principles of pulse electron paramagnetic resonance*. Oxford University Press, 2001.
- [6] Mark C. Butler and Daniel P. Weitekamp. Polarization of nuclear spins by a cold nanoscale resonator. *Physical Review A*, 84(6):063407, December 2011.
- [7] Christopher J. Wood, Troy W. Borneman, and David G. Cory. Cavity Cooling of an Ensemble Spin System. *Physical Review Letters*, 112(5):050501, February 2014.
- [8] A. Abragam. *The Principles of Nuclear Magnetism*. Clarendon Press, Oxford, 1961.
- [9] A. Einstein. Strahlungs-emission und absorption nach der quantentheorie. *Verhandlungen der Deutschen Physikalischen Gesellschaft*, 18:318, 1916.
- [10] S. Haroche and J.-M. Raimond. *Exploring the quantum*. Oxford University Press, August 2006.
- [11] G. Feher and E. A. Gere. Electron Spin Resonance Experiments on Donors in Silicon. II. Electron Spin Relaxation Effects. *Physical Review*, 114(5):1245–1256, June 1959.
- [12] Alexei M. Tyryshkin, Shinichi Tojo, John J. L. Morton, Helge Riemann, Nikolai V. Abrosimov, Peter Becker, Hans-Joachim Pohl, Thomas Schenkel, Michael L. W. Thewalt, Kohei M. Itoh, and S. A. Lyon. Electron spin coherence exceeding seconds in high-purity silicon. *Nature Materials*, 11(2):143–147, 2012.
- [13] G. Feher. Electron Spin Resonance Experiments on Donors in Silicon. I. Electronic Structure of Donors by the Electron Nuclear Double Resonance Technique. *Phys. Rev.*, 114(5):1219–1244, June 1959.
- [14] M. H. Mohammady, G. W. Morley, and T. S. Monteiro. Bismuth Qubits in Silicon: The Role of EPR Cancellation Resonances. *Physical Review Letters*, 105(6), August 2010.
- [15] C. Macklin, K. OBrien, D. Hover, M. E. Schwartz, V. Bolkhovskiy, X. Zhang, W. D. Oliver, and I. Siddiqi. A nearquantum-limited Josephson traveling-wave parametric amplifier. *Science*, 350(6258):307–310, October 2015.
- [16] Zhixin Wang, Mingrui Xu, Xu Han, Wei Fu, Shruti Puri, S. M. Girvin, Hong X. Tang, S. Shankar, and M. H. Devoret. Quantum Microwave Radiometry with a Superconducting Qubit. *arXiv:1909.12295 [quant-ph]*, September 2019.
- [17] Mingrui Xu, Xu Han, Chang-Ling Zou, Wei Fu, Yuntao Xu, Changchun Zhong, Liang Jiang, and Hong X. Tang. Radiative cooling of a superconducting resonator. *arXiv:1910.01203 [quant-ph]*, October 2019. arXiv: 1910.01203.
- [18] Richard E. George, Wayne Witzel, H. Riemann, N. V. Abrosimov, N. Ntzel, Mike L. W. Thewalt, and John J. L. Morton. Electron Spin Coherence and Electron Nuclear Double Resonance of Bi Donors in Natural Si. *Physical Review Letters*, 105(6):067601, August 2010.
- [19] M. Pechal, J.-C. Besse, M. Mondal, M. Oppliger, S. Gasparinetti, and A. Wallraff. Superconducting Switch for Fast On-Chip Routing of Quantum Microwave Fields. *Physical Review Applied*, 6(2):024009, August 2016.
- [20] Lewis A. Williamson, Yu-Hui Chen, and Jevon J. Longdell. Magneto-Optic Modulator with Unit Quantum Efficiency. *Physical Review Letters*, 113(20):203601, November 2014.
- [21] Mario F. Gely, Marios Kounalakis, Christian Dickel, Jacob Dalle, Rmy Vatr, Brian Baker, Mark D. Jenkins, and Gary A. Steele. Observation and stabilization of photonic Fock states in a hot radio-frequency resonator. *Science*, 363(6431):1072–1075, March 2019.
- [22] W. Rauch, E. Gornik, G. Slkner, A. A. Valenzuela, F. Fox, and H. Behner. Microwave properties of YBa2cu3o7x thin films studied with coplanar transmission line resonators. *Journal of Applied Physics*, 73(4):1866–1872, February 1993.
- [23] Frank J. Adrian. Theory of Anomalous Electron Spin Resonance Spectra of Free Radicals in Solution. Role of Diffusion-Controlled Separation and Reencounter of Radical Pairs. *The Journal of Chemical Physics*, 54(9):3918–3923, May 1971.
- [24] S. K. Wong, D. A. Hutchinson, and J. K. S. Wan. Chemically induced dynamic electron polarization. II. A general theory for radicals produced by photochemical reactions of excited triplet carbonyl compounds. *The Journal of Chemical Physics*, 58(3):985–989, February 1973.
- [25] M. Steger, K. Saeedi, M. L. W. Thewalt, J. J. L. Morton, H. Riemann, N. V. Abrosimov, P. Becker, and H.-J. Pohl. Quantum Information Storage for over 180 s Using Donor Spins in a 28si Semiconductor Vacuum. *Science*, 336(6086):1280–1283, August 2012.
- [26] Marcus W. Doherty, Neil B. Manson, Paul Delaney, Fedor Jelezko, Jrg Wrachtrup, and Lloyd C. L. Hollenberg. The nitrogen-vacancy colour centre in diamond. *Physics Reports*, 528(1):1–45, July 2013.
- [27] J. G. Castle and D. W. Feldman. Resonance Modes at Defects in Crystalline Quartz. *Physical Review*, 137(2A):A671–A673, January 1965.
- [28] Jean-Pierre Gayda, Patrick Bertrand, Alain Deville, Claude More, Guy Roger, John F. Gibson, and R. Cammack. Temperature dependence of the electronic spin-lattice relaxation time in a 2-iron-2-sulfur protein. *Biochimica et Biophysica Acta (BBA) - Protein Structure*, 581(1):15–26, November 1979.
- [29] Yi Zhou, Bruce E. Bowler, Gareth R. Eaton, and Sandra S. Eaton. Electron Spin Lattice Relaxation Rates for S = 12 arXiv: 1909.12295.

Molecular Species in Glassy Matrices or Magnetically Dilute Solids at Temperatures between 10 and 300 K. *Journal of Magnetic Resonance*, 139(1):165–174, July 1999.

- [30] S. Probst, A. Bienfait, P. Campagne-Ibarcq, J. J. Pla, B. Albanese, J. F. Da Silva Barbosa, T. Schenkel, D. Vion, D. Esteve, K. M. Imer, J. J. L. Morton, R. Heeres, and P. Bertet. Inductive-detection electron-spin resonance spectroscopy with $65 \text{ spins/Hz}^{1/2}$ sensitivity. *Applied Physics Letters*, 111(20):202604, 2017.
- [31] T. Sekiguchi, M. Steger, K. Saeedi, M. L. W. Thewalt, H. Riemann, N. V. Abrosimov, and N. Ntzel. Hyperfine Structure and Nuclear Hyperpolarization Observed in the Bound Exciton Luminescence of Bi Donors in Natural Si. *Physical Review Letters*, 104(13):137402, April 2010.
- [32] Vishal Ranjan, Sebastian Probst, Bartolo Albanese, Andrin Doll, Oscar Jacquot, Emmanuel Flurin, Reinier Heeres, Denis Vion, Daniel Esteve, John Morton, and Patrice Bertet. Pulsed electron spin resonance spectroscopy in the Purcell regime. *arXiv:1909.02443 [cond-mat]*, September 2019. arXiv: 1909.02443.

SUPPLEMENTARY INFORMATION

Thermalization of a system coupled to N bosonic baths.

When a physical system exchanges energy with an environment consisting of N reservoirs at different temperatures T_j , the intermediate effective temperature T_{sys} at which the system equilibrates depends on the strength Γ_j with which it is coupled to each bath, defined as the rate at which the system would spontaneously relax from its first excited to its ground state by emitting a quantum of energy into this bath at zero temperature. For a system coupled to N bosonic reservoirs, T_{sys} is obtained by

$$\bar{n}(T_{\text{sys}}) = \sum_{j=1}^N (\Gamma_j/\Gamma) \bar{n}(T_j), \quad (1)$$

$\bar{n}(T) = 1/[1 - \exp^{-\hbar\omega_0/kT}]$ being the occupation number of a bosonic mode at frequency ω_0 , and $\Gamma = \sum_{j=1}^N \Gamma_j$ the total system-bath coupling. If the system is dominantly coupled to one bath j_0 ($\Gamma_{j_0} \gg \Gamma_{j \neq j_0}$), the system therefore equilibrates close to T_{j_0} regardless of the temperature of the other reservoirs.

Cavity thermal photon population. The resonator mode of frequency ω_0 is coupled by internal dissipation of rate κ_{int} to a hot thermal bath at T_{int} , not necessarily equal to the sample temperature T_{phon} , and by the external losses of rate κ_{ext} , to the thermal radiation in the propagating input mode, whose temperature T_{ext} is determined by the switch state. From Eq.1 we get $\bar{n}(T_{\text{phot}}) = (\kappa_{\text{int}}/\kappa)\bar{n}(T_{\text{int}}) + (\kappa_{\text{ext}}/\kappa)\bar{n}(T_{\text{ext}})$, where $\kappa = \kappa_{\text{int}} + \kappa_{\text{ext}}$. In the same way, when the switch is in the *cold* configuration, the input mode is coupled to the cold bath at T_{cold} and, as a consequence of losses and impedance mismatches modeled by the absorption factor α , to the hot bath at T_{phon} . The thermal occupation of the input mode at ω_0 in the *cold* state is then an average of the hot and cold bath populations expressed as $\bar{n}(T_{\text{ext}}^{\text{cold}}) = (1 - \alpha)\bar{n}(T_{\text{cold}}) + \alpha\bar{n}(T_{\text{phon}})$. In the present experiment $T_{\text{cold}} = 20$ mK, therefore $\bar{n}(T_{\text{cold}}) \approx 0$. Substituting $\bar{n}(T_{\text{ext}}^{\text{cold}})$ in the expression of $\bar{n}(T_{\text{phot}})$, the average number of resonator thermal photons in the *cold* case is found to be $\bar{n}(T_{\text{phot}}^{\text{cold}}) \approx \frac{\kappa_{\text{int}}}{\kappa}\bar{n}(T_{\text{int}}) + \frac{\alpha\kappa_{\text{ext}}}{\kappa}\bar{n}(T_{\text{phon}})$. When in *hot*, $\bar{n}(T_{\text{ext}}^{\text{hot}}) = \bar{n}(T_{\text{phon}})$ and $\bar{n}(T_{\text{phot}}^{\text{hot}}) = (\kappa_{\text{int}}/\kappa)\bar{n}(T_{\text{int}}) + (\kappa_{\text{ext}}/\kappa)\bar{n}(T_{\text{phon}})$.

Spin effective temperature T_{spin} and cooling factor η . The spins are coupled with strength Γ_{phot} to the resonator mode populated by $\bar{n}(T_{\text{phot}})$ thermal photons, and with strength Γ_{phon} to the lattice phonon mode of occupation number $\bar{n}(T_{\text{phon}})$. From Eq.1, the spin temperature is defined as $\bar{n}(T_{\text{spin}}) = [\Gamma_{\text{phon}}/(\Gamma_{\text{phon}} + \Gamma_{\text{phot}})]\bar{n}(T_{\text{phon}}) + [\Gamma_{\text{phot}}/(\Gamma_{\text{phon}} + \Gamma_{\text{phot}})]\bar{n}(T_{\text{phot}})$. As discussed in the main text for the Purcell rate, a spin coupled to a bosonic mode of temperature T_j with strength Γ_j relaxes at a rate $\Gamma_1 = \Gamma_j[2\bar{n}(T_j) + 1]$ as a consequence of absorption and emission rate dependence on the thermal population of the mode. The relaxation rate of

the spins coupled to the effective bath of temperature T_{spin} is then $\Gamma_1 = (\Gamma_{\text{phon}} + \Gamma_{\text{phot}})[2\bar{n}(T_{\text{spin}}) + 1] = \Gamma_{\text{phon}}[2\bar{n}(T_{\text{phon}}) + 1] + \Gamma_{\text{phot}}[2\bar{n}(T_{\text{phot}}) + 1]$, that is the sum of the spin-photon and spin-lattice relaxation rates, as expected. On the other hand, the polarization of the spins at temperature T_{spin} is $p(T_{\text{spin}}) = 1/[2\bar{n}(T_{\text{spin}}) + 1] = (\Gamma_{\text{phon}}/\Gamma_1)p(T_{\text{phon}}) + (\Gamma_{\text{phot}}/\Gamma_1)p(T_{\text{phot}})$, so equal to the equilibrium polarizations at the two baths temperatures weighted by the corresponding relaxation rates. The cooling factor, defined as the ratio of the equilibrium polarization in the two switch states, is therefore still equal to the ratio of total relaxation rates as for purely Purcell relaxation, $\eta = \frac{\Gamma_{\text{phon}}(2\bar{n}(T_{\text{phon}})+1)+\Gamma_{\text{phot}}(2\bar{n}(T_{\text{phot}}^{\text{hot}})+1)}{\Gamma_{\text{phon}}(2\bar{n}(T_{\text{phon}})+1)+\Gamma_{\text{phot}}(2\bar{n}(T_{\text{phot}}^{\text{cold}})+1)}$. In this work we assume Γ_{phon} to be negligible in the absence of infrared radiation from the LED, as confirmed by the resonator mode temperature measurement and by simulation of the Purcell decay. In the model used to fit $\eta(I)$ in Fig. 4b, we neglect a possible effect of illumination on the lattice bath temperature.

Measurement of cavity mode temperature. Measuring the noise power spectral density S in the output mode yields an estimate of the resonator mode temperature. $S(\omega, T_{\text{phon}})$ has then been measured in a 6 MHz bandwidth around ω_0 for T_{phon} ranging from 840 mK to 1.16 K in both switch configurations. A lower resonator quality factor in the *cold* than in the *hot* configuration, measured at $B_0 = 0$, points to a reduced temperature of the internal losses $T_{\text{int}}^{\text{cold}} < T_{\text{int}}^{\text{hot}}$ possibly due to cooling of the electric dipoles coupled to the resonator. We therefore consider the general case of resonator internal losses temperature $T_{\text{int}} \neq T_{\text{phon}}$. In the *h* configuration then, $S^{\text{hot}}/G(\omega)\hbar\omega = [1 - \beta(\omega)]\bar{n}(T_{\text{phon}}) + \beta(\omega)\bar{n}(T_{\text{int}}^{\text{cold}}) + 1/2 + n_{\text{TWPA}}$, where $G(\omega)$ is the known frequency-dependent total gain of the output line, n_{TWPA} the noise added by the TWPA and $\beta(\omega) = 4\kappa_{\text{int}}\kappa_{\text{ext}}/(\kappa^2 + 4(\omega - \omega_0)^2)$ the transmission function. On the other hand, the expression of S in the *cold* case is $S^{\text{cold}}/G(\omega)\hbar\omega = [\alpha(1 - \beta(\omega))]\bar{n}(T_{\text{phon}}) + \beta(\omega)\bar{n}(T_{\text{int}}^{\text{cold}}) + 1/2 + n_{\text{TWPA}}$. A first fit of $S^{\text{hot}}(T_{\text{phon}})$ gives $n_{\text{TWPA}} = 0.75 \pm 0.25$. By then fitting $S^{\text{hot}}(\omega)$ for each value of T_{phon} we obtain the corresponding $T_{\text{int}}^{\text{hot}}$, while α and $T_{\text{int}}^{\text{cold}}$ result from the fit of $S^{\text{cold}}(\omega)$. The temperature T_{int} of the resonator internal losses is found to be about 10% larger (lower) than T_{phon} values in the *hot* (*cold*) configuration. For all T_{phon} values we extract $\alpha \simeq 0.47 \pm 0.1$. The extracted parameters allow to calculate the cavity thermal photon population using $\bar{n}(T_{\text{phot}}^{\text{hot}}) = (\kappa_{\text{ext}}/\kappa)\bar{n}(T_{\text{phon}}) + (\kappa_{\text{int}}/\kappa)\bar{n}(T_{\text{int}}^{\text{hot}})$ and $\bar{n}(T_{\text{phot}}^{\text{cold}}) = \alpha(\kappa_{\text{ext}}/\kappa)\bar{n}(T_{\text{phon}}) + (\kappa_{\text{int}}/\kappa)\bar{n}(T_{\text{int}}^{\text{cold}})$ in the *hot* and *cold* configuration, respectively. The effective intra-cavity field temperature of $T_{\text{phot}}^{\text{hot}} = 850$ mK and $T_{\text{phot}}^{\text{cold}} = 500 \pm 60$ mK are then found at $T_{\text{phon}} = 840$ mK, corresponding to a predicted cooling factor $\eta = 1.65 \pm 0.2$ for the spins. The measurement of S therefore confirms that the spin cooling efficiency is limited by the temperature of the intra-cavity mode rather than non-radiative spin relaxation phenomena.

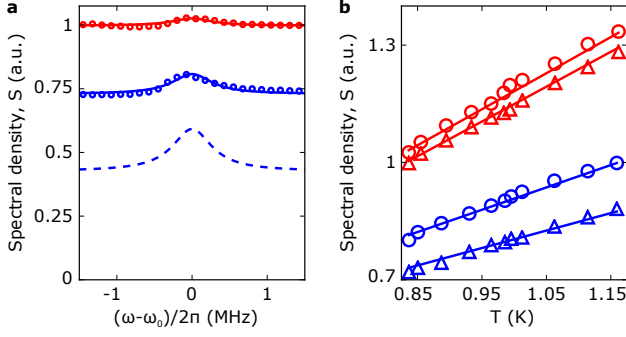


FIG. 5. **Noise power spectral density measurement.** **a**, Frequency dependence of the noise power spectral density S measured at $T_{spl} = 840$ mK for the h (red circles) and c (blue circles) switch configurations. Hot data are fitted with $S^h/\hbar\omega = G(\omega)((1 - \beta(\omega))\bar{n}(T_{spl}) + \beta(\omega)\bar{n}(T_i^h) + 1/2 + n_{TWPA})$ (solid red line), fixing $n_{TWPA} = 0.75 \pm 0.25$ and obtaining $T_i^h = 950$ mK as the only free parameter. From the fit of the cold data with $S^c/\hbar\omega = G(\omega)(\alpha(1 - \beta(\omega))\bar{n}(T_{spl}) + \beta(\omega)\bar{n}(T_i^c) + 1/2 + n_{TWPA})$ (solid blue line), $\alpha = 0.47 \pm 0.04$ and $T_{int}^{cold} = 760$ mK are obtained. The blue dashed line indicates the expected $S^{cold}(\omega)$ for $\alpha = 0$. **b**, Still temperature T_{phon} dependence of S measured at $\omega = \omega_0$ (open circles) and at $\omega - \omega_0 = -2.7$ MHz (open triangles) for both *hot* (red) and *cold* (blue) configurations. Solid lines are plot of S^{hot} (red) and S^{cold} (blue) with parameters obtained from the frequency dependence fits performed at all T_{phon} , and with $n_{TWPA} = 0.75$.

Bismuth donors in silicon. The spin Hamiltonian of bismuth donors in silicon includes a Zeeman effect and an isotropic hyperfine coupling: $H/\hbar = \mathbf{B} \cdot (\gamma_e \mathbf{S} \otimes \mathbb{1} - \gamma_n \mathbb{1} \otimes \mathbf{I}) + A \mathbf{S} \cdot \mathbf{I}$, where $\gamma_e/2\pi = 27.997$ GHz is the electronic gyromagnetic ratio, $\gamma_n/2\pi = 6.9$ MHz is the nuclear gyromagnetic ratio and $A/\hbar = 1.475$ GHz is the hyperfine coupling constant. For low applied static magnetic field aligned along z ($B_0 \gamma_e \lesssim A$), the eigenstates of \mathbf{S} and \mathbf{I} are highly hybridized and the energy eigenbasis is $|F, m\rangle$, in which $\mathbf{F} = \mathbf{S} + \mathbf{I}$ is the total angular momentum of eigenvalue F and F_z its projection along \mathbf{B}_0 with eigenvalue m . An oscillating field along x or y can therefore excite transitions satisfying $\Delta F \Delta m = \pm 1$, whose matrix elements $\langle F, m | S_x | F + 1, m \pm 1 \rangle = \langle F, m | S_y | F + 1, m \pm 1 \rangle$ are comparable in magnitude with the ideal electronic spin 1/2 transition $\langle -1/2 | S_x | 1/2 \rangle = 0.5$. We note here that in the $-4 < m \leq 4$ manifold the $|F, m - 1\rangle \leftrightarrow |F + 1, m\rangle$ and $|F, m\rangle \leftrightarrow |F + 1, m - 1\rangle$ transitions are quasi degenerate in frequency and the sum of their associated S_x matrix elements is equal to 0.5. The spectrum consists then of 6 resolvable transitions for $B_0 < 100$ mT, as shown in Fig. 1.c. At zero field the 9 ground ($F = 4$) and 11 excited ($F = 5$) multiplets are separated by a frequency of 7.38 GHz. For B_0 going from 0 to 65 mT, the hyperfine splitting within the two multiplets $E_{hyp} = E_{|F, m+1\rangle} - E_{|F, m\rangle}$ increases from 0 to about 150 MHz.

Population difference $\Delta N(T)$ for bismuth donors. The magnetic resonance signal is proportional to the population unbalance $\Delta N = N_\uparrow - N_\downarrow$, where N_\uparrow (N_\downarrow) is the total num-

ber of spins in the excited (ground) state of the spin transition considered. In the case of bismuth donors, where the electron spin transitions $|4, m\rangle \leftrightarrow |5, m - 1\rangle$ and $|4, m - 1\rangle \leftrightarrow |5, m\rangle$ (for $-4 < m \leq 4$) are quasi-degenerate in frequency compared to resonator linewidth, $\Delta N(T_{spin})$ is the population unbalance between the two excited and the two ground states: $\Delta N(T_{spin}) = N(p_{|4, m\rangle} + p_{|4, m-1\rangle} - p_{|5, m\rangle} - p_{|5, m-1\rangle})$, where N is the total number of donors, and $p_{|F, m\rangle} = e^{-E_{F, m}/kT_{spin}}/Z$ is the occupation probability of $|F, m\rangle$, with $Z = \sum_{F, m} e^{-E_{F, m}/kT_{spin}}$ the partition function. The green line in Fig.2 of the main text shows $\Delta N(T)$ for the transition considered.

As long as $T_{spin} > 100$ mK and $B_0 < 70$ mT, the thermal energy is much larger than the energy difference between hyperfine states of both $F = 5$ and $F = 4$ manifolds $E_{|F, m\rangle} - E_{|F, m-1\rangle}$. In that case, one can show that $\Delta N(T_{spin}) \simeq \frac{N}{9} \frac{1 + e^{-\hbar\omega_0/kT_{spin}}}{1 + 11/9 e^{-\hbar\omega_0/kT_{spin}}} \tanh(\hbar\omega_0/2kT_{spin})$, which can be approximated by $\frac{N}{10} \tanh(\hbar\omega_0/2kT_{spin})$ especially when $kT_{spin} > \hbar\omega_0$, which happens in our case for $T_{spin} > 300$ mK. This is visible in Fig. 2c, where the computed $\Delta N(T)$ (green curve) indeed coincides well with the result for a spin-1/2 $\tanh(\hbar\omega_0/2kT_{spin})$ (red curve) for $T_{spin} > 300$ mK (by proper choice of the scale for A_e).

Temperature dependence of polarization for transitions $|4, -1\rangle \leftrightarrow |5, 0\rangle$ and $|4, 0\rangle \leftrightarrow |5, -1\rangle$. We first measure the temperature dependence of polarisation at $B_0 = 62.5$ mT waiting several hours at each temperature value before measuring the echo amplitude A_e . The result reported in Fig. 5 (red circles) shows a significant deviation below 200 mK from the calculated $\Delta N(T)$ (red line). Spins are then in a non-thermal state below 200 mK, possibly due to residual infrared radiation reaching the sample. This is known to cause redistribution of population in the bismuth hyperfine levels [31]. We repeat then the same measurement by adding at each temperature point a first step during which we set $B_0 = 9.3$ mT for 20 min before setting the field back to 62.5 mT. 4 min after the field is set to 62.5 mT, we measure A_e . The result is reported in both Fig. 1c (green dots) and Fig. 6 (black circles) and is in good agreement with the calculated $\Delta N(T)$ for the same transitions and $B_0 = 9.3$ mT. This shows that at lower field the spins reach thermal equilibrium while the depolarising phenomenon taking place at 62.5 mT is not effective. In a third measurement performed at $T = 83$ mK we first set $B_0 = 9.3$ mT during 20 min, then we set $B_0 = 62.5$ mT and immediately after we record continuously A_e as a function of time. The result reported in the inset of Fig. 6 shows the spins reaching the equilibrium non-thermal state in the time-scale of hours, orders of magnitude longer than the 4 min waiting time used to detect the thermal equilibrium polarization after field sweep from 9.3 mT to 62.5 mT.

Estimate of single spin coupling g . The interaction of the individual bismuth donor spins with the resonator mode of frequency ω_0 is described by the Jaynes-Cummings Hamil-

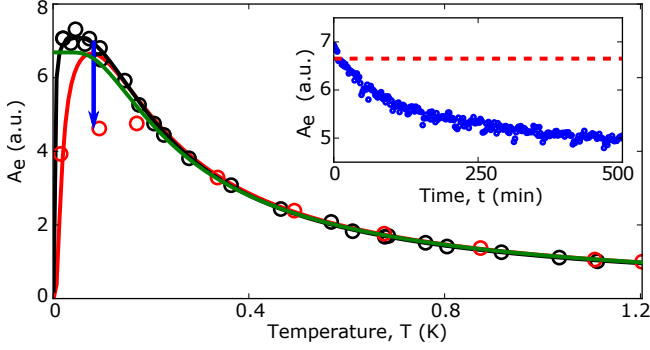


FIG. 6. **Temperature dependence of polarization for transitions** $|4, -1\rangle \leftrightarrow |5, 0\rangle$ and $|4, 0\rangle \leftrightarrow |5, -1\rangle$. Equilibrium polarization of transitions $|4, -1\rangle \leftrightarrow |5, 0\rangle$ and $|4, 0\rangle \leftrightarrow |5, -1\rangle$ measured at $B_0 = 62.5$ mT (red circles). Several hours are waited at each temperature before recording A_e . Red line is the calculated $\Delta N(T)$ for the considered transition at $B_0 = 62.5$ mT. A second polarisation measurement of the same transitions (black circles) is reported. In this experiment, for each temperature value, B_0 is first set to 9.3 mT during 20 min, then it is set to 62.5 mT and finally after 4 min A_e is recorded. The black line is the calculated $\Delta N(T)$ for the considered transition at $B_0 = 9.3$ mT. The polarisation $p(T) = \tanh(\hbar\omega_0/kT)$ of a spin 1/2 is also shown for comparison (green). A_e as a function of time (inset) is also shown for $T = 83$ mK and $B_0 = 62.5$ mT after B_0 has been set to 9.3 mT for 20 min. The same data are represented in the main plot with the blue arrow.

tonian $H = \hbar g(\sigma^+ a + \sigma^- a^\dagger)$, where σ^+ (σ^-) is the spin raising (lowering) operator, a (a^\dagger) is the annihilation (creation) operator for intra-cavity photons, and g is the spin-photon coupling strength. All the spin echo measurement in the present work, unless specified, are performed at 62.5 mT on the $|4, -1\rangle \leftrightarrow |5, 0\rangle$ and $|4, 0\rangle \leftrightarrow |5, -1\rangle$ quasi-degenerate transitions whose matrix elements are equal to 0.28 and 0.22, respectively. As a consequence, two families of spins are probed simultaneously, with different coupling strengths given by $g = \gamma_e \langle F, m | S_y | F + 1, m - 1 \rangle |\delta B_1|$, where δB_1 is the magnitude of the magnetic field vacuum fluctuations at the spin location generated by the current vacuum fluctuations δi in the resonator inductor wire. The value of δi is given by $\delta i = \omega_0 \sqrt{\hbar/2Z_0}$, where $Z_0 = \sqrt{L/C} = 46 \Omega$ is the characteristic impedance of the LC resonator estimated from electromagnetic simulation realized in CST Microwave studio. In order to obtain δB_1 in the silicon substrate around the inductor, we perform simulation of the magnetic field generated by δi using COMSOL software. A non-uniform distribution of the current density in the superconducting niobium wire is assumed. The so obtained spatial distribution of the coupling constant $g(x, y)$ for the $|4, 0\rangle \leftrightarrow |5, -1\rangle$ transition is shown in Fig. 1b. Combining $g(x, y)$ for the two transitions with the spin implantation profile (see Fig. 1b), we extract the coupling distribution density of the spin ensemble $\rho(g)$ (see Fig. 7a) that we use in the spin simulation to reproduce

the Hahn echo measurements.

Spin simulation. The simulation of the dynamics of the spin ensemble weakly coupled to the intra-cavity field consists in numerical solution of the system semi-classical equation of motion, as described in [32]. The system of differential equations is solved for M values of coupling g and the results are averaged using $\rho(g)$ as weighting function. The transverse relaxation time is fixed to the measured T_2 while the longitudinal relaxation rate is imposed for each g value to be the Purcell rate: $\Gamma_1 = \frac{\kappa g^2}{k^2/4 + \delta^2}$, where $\delta = \omega_s - \omega_0$ is the spin-cavity detuning. The spin distribution in frequency is modeled as a square centered at ω_0 and 3 MHz wide. Simulation of Rabi oscillations driven by varying the amplitude of the second pulse in Hahn echo sequence is shown in Fig. 7b. The average of signals emitted by spins with different Rabi frequencies results in damped oscillations that are in qualitative agreement with the experimental data. The pulse amplitude giving the maximum signal is then chosen as π pulse amplitude for the simulation of the inversion recovery sequence.

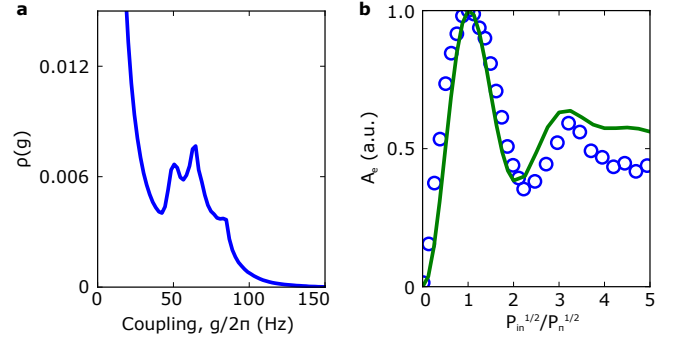


FIG. 7. **Simulation of Rabi oscillations.** **a**, Distribution of the spin-cavity coupling g obtained from the spatial distribution of δB_1 . **b**, Rabi oscillations measured at $B_0 = 62.5$ mT and $T = 15$ mK by varying the amplitude of the second pulse in the Hahn echo sequence (blue circles). The pulse amplitude is normalized to the value $P_\pi^{1/2}$ corresponding to the maximum in detected signal. The solid green line is the result of the numerical simulation of a spin ensemble described by $\rho(g)$.

Pulse sequences. All the A_e data points presented in this work, excepted the SNR measurement, are obtained using an Hahn echo sequence followed by a Carr-Purcell-Meiboom-Gill sequence (CPMG). From 100 to 300 π pulse are therefore applied after the first echo to record as many additional echoes, that are then averaged to improve the signal-to-noise ratio. The π pulse length is fixed to 250 ns and double with respect to the $\pi/2$ pulse. The amplitude of the two pulses is always the same while the phase of the π pulses is 90° shifted. The spectrum presented in Fig. 1d is measured with a delay $\tau = 8 \mu\text{s}$ between the $\pi/2$ pulse and the π pulse, 10 additional CPMG π pulses separated by $16 \mu\text{s}$ and a repeti-

tion time t_{rep} of 5.8 s. The measurement is averaged 32 times at each B_0 field value. The Γ_1 measurements of Fig. 2 are realized with $\tau = 15 \mu\text{s}$, 300 CPMG pulses separated by 2τ , $t_{rep} = 80$ s. At each temperature the Γ_1^{-1} measurement is repeated 8 times and then averaged. The echo amplitude as a function of temperature shown in Fig. 2c is obtained with $\tau = 15 \mu\text{s}$, $t_{rep} = 120$ s, 300 CPMG pulses separated by 2τ and no further averaging. For the Γ_1 measurement of Fig. 3 $\tau = 15 \mu\text{s}$, $t_{rep} = 120$ s, 100 CPMG pulses are separated by 2τ and no further averaging is used. In the T_2 experi-

ment of Fig. 3c, $t_{rep} = 10$ s, 300 CPMG pulses separated by $8 \mu\text{s}$ are used and each data point is averaged 4 times. The pulse sequence of each echo sample in the SNR experiment of Fig. 3d does not include CPMG and has $\tau = 15 \mu\text{s}$. Fig. 4a shows results of Γ_1 measurements realized with $\tau = 15 \mu\text{s}$, $t_{rep} = 40$ s, 300 CPMG pulses separated by 2τ . At each LED I the Γ_1 measurement is repeated 4 times and then averaged. The cooling and recovery dynamics of Fig. 4b are instead measured using $\tau = 19.5 \mu\text{s}$, $t_{rep} = 30$ s, 100 CPMG pulses separated by 2τ and 20 averages of each data point.